

Local MDI+: Local Feature Importances for Tree-Based Models

Zhongyuan Liang*

Department of Computational Precision Health
UC Berkeley and UCSF
zhongyuan_liang@berkeley.edu

Zachary T. Rewolinski*

Department of Statistics
UC Berkeley
zachrewolinski@berkeley.edu

Abhineet Agarwal

Department of Statistics
UC Berkeley
aa3797@berkeley.edu

Tiffany M. Tang

Department of Applied and Computational Mathematics and Statistics
University of Notre Dame
ttang4@nd.edu

Bin Yu

Department of Statistics and EECS
UC Berkeley
binyu@berkeley.edu

Abstract

Tree-based ensembles such as random forests remain the go-to for tabular data over deep learning models due to their prediction performance and computational efficiency. These advantages have led to their widespread deployment in high-stakes domains, where interpretability is essential for ensuring trustworthy predictions. This has motivated the development of popular local (i.e. sample-specific) feature importance (LFI) methods such as LIME and TreeSHAP. However, these approaches rely on approximations that ignore the model’s internal structure and instead depend on potentially unstable perturbations. These issues are addressed in the global setting by MDI+, a feature importance method which exploits an equivalence between decision trees and linear models on a transformed node basis. However, the global MDI+ scores are not able to explain predictions when faced with heterogeneous individual characteristics. To address this gap, we propose Local MDI+ (LMDI+)¹, a novel extension of the MDI+ framework to the sample-specific setting. LMDI+ outperforms existing baselines LIME and TreeSHAP in identifying instance-specific signal features, averaging a 10% improvement in downstream task performance across twelve real-world benchmark datasets. It further demonstrates greater stability by consistently producing similar instance-level feature importance rankings across multiple random forest fits. Finally, LMDI+ enables local interpretability use cases, including the identification of closer counterfactuals and the discovery of homogeneous subgroups.

*Equal contribution

¹LMDI+ is integrated into the `imodels` package <https://github.com/csinva/imodels> [1]. Experimental results can be found at <https://github.com/Yu-Group/imodels-experiments>.

1 Introduction

Despite the growing diversity of data types in various fields, tabular data continues to be one of the most prevalent and widely utilized formats in real-world applications. Tree-based models such as random forests (RFs) and gradient boosting (GB) [2, 3] have consistently demonstrated state-of-the-art performance and computational efficiency on tabular datasets, often outperforming deep learning-based algorithms [4, 5]. Consequently, tree-based models are frequently deployed in high-stakes environments such as healthcare [6–8] and criminal justice [9–11].

However, the use of algorithms to automate decision-making raises concerns about safety, making trustworthy interpretations necessary for deployment in critical settings. Local feature importance (LFI) methods play a central role in this effort by identifying influential features that drive each observation’s prediction. Among LFI methods, LIME (Local Interpretable Model-agnostic Explanations) and SHAP (Shapley Additive Explanations) [12, 13] remain the most widely used approaches for tree-based models and have been applied in various fields [14, 15].

Despite the prevalence of these methods, researchers have demonstrated significant limitations [16–20]. In particular, their model-agnostic nature requires measuring changes in predictions of perturbed inputs rather than utilizing the inner model structure. Specifically, LIME generates random perturbations around each instance and provides explanations by fitting a sparse linear model over the predicted responses. Similarly, SHAP approximates the change in model output by perturbing feature inclusion across all possible subsets. While such model-agnostic methods are useful when the model internals are inaccessible, they may overlook structural information that can produce more faithful explanations. Furthermore, they often fail to identify the true signal features in the data-generating process (DGP) [16, 18] and produce unstable feature importances [17, 19].

Another common avenue for interpreting tree-based models is mean decrease in impurity (MDI). MDI quantifies global feature importances by computing the average reduction in impurity (e.g. Gini or entropy) resulting from splitting on each feature. However, MDI has well-documented biases towards features with high entropy or low correlation [21, 22]. The MDI+ framework generates global feature importances which reduce these biases through an enhanced data representation and regularization [23]. Due to their global nature, the resulting feature importance scores cannot be used to explain sample-specific outcomes which often depend on unique individual characteristics. To address this gap, we propose Local MDI+ (LMDI+), a novel extension of the MDI+ framework to the sample-specific setting. LMDI+ inherits the strengths of MDI+ while addressing shortcomings of existing LFI methods by more faithfully and consistently identifying signal features in the underlying data-generating process (DGP). In this work, we demonstrate that LMDI+ accomplishes the following:

1. **Identifies signal.** We perform synthetic experiments to show that LMDI+ achieves state-of-the-art performance in identifying signal features across DGPs, noise levels, and correlation levels.
2. **Captures predictive features.** We conduct real-world experiments on multiple benchmark datasets to demonstrate that LMDI+ outperforms existing methods in detecting features that are more predictive of individual outcomes.
3. **Ensures stability.** Stability experiments show that LMDI+ identifies consistent sample-wise influential features, demonstrating superior stability compared to baseline methods.
4. **Enhances practical applications.** We show that LMDI+ strengthens meaningful applications of LFIs, such as finding better counterfactual explanations and discovering subgroups which simplify the underlying prediction task.

2 Related Work

Tree-based models. Tree-based models offer a straightforward rule-based approach to prediction and are renowned for their exceptional performance and computational efficiency [2, 24, 4]. The most popular decision tree algorithm is CART (classification and regression trees), which generates predictions using a single tree [25]. Tan et al. [26] propose FIGS, an extension of CART which improves upon prediction performance by accounting for additive structure. However, individual trees are weak learners [27] and thus tend to underperform on complex tasks [28]. Ensemble methods, such as RFs [2] and variants including generalized RFs [29] and iterative RFs [30], seek to enhance predictive performance by aggregating multiple trees trained on bootstrapped samples of data.

Global feature importance. Global feature importance methods summarize the overall contributions of features across the entire dataset. Mean decrease in impurity (MDI) [25] is the most widely-used feature importance method for tree-based models. MDI assigns importance to a feature k according to the decrease in impurity resulting from nodes splitting on k . However, MDI is known to favor features with high entropy or low correlation with other features, regardless of their relationship with the outcome [21, 22]. The MDI+ framework [23] explains these drawbacks by providing a reinterpretation of MDI as an R^2 value in an equivalent linear regression. MDI+ furthermore addresses these drawbacks and generalizes MDI by using regularized generalized linear models (GLMs) and appending smooth features to the equivalent linear representation.

Local feature importance. Local feature importances attempt to explain individual predictions, providing values for each observation rather than for the model as a whole. LIME and SHAP are two popular LFI methods which are often used to explain tree-based models. LIME generates random perturbations around each instance and provides explanations by fitting a sparse linear model over the predicted responses [12]. However, this reliance on random perturbations introduces significant instability due to randomness in the sampling process [17, 19, 20]. SHAP, inspired by game-theoretic Shapley values, approximates the average contribution of a feature across all possible feature permutations [13]. TreeSHAP improves the computational efficiency of this process for tree-based models [31]. However, SHAP and TreeSHAP have been found to fail to identify signal features and can yield misleading feature importance rankings [18]. Moreover, in certain provable cases, they have been shown to perform no better than random guessing [16].

3 The Local MDI+ Framework

This section introduces the LMDI+ framework for local feature importance. We begin with a brief review of MDI and subsequently highlight the connection between MDI and the R^2 metric from linear regression, giving rise to MDI+. We then further exploit this linear regression interpretation of MDI by extending the MDI+ framework for global feature importance to the sample-specific setting.

3.1 Mean Decrease in Impurity

Let dataset $\mathcal{D} = \{(\mathbf{x}_i, y_i)\}_{i=1}^n$ be given, with covariates $\mathbf{x}_i \in \mathbb{R}^p$ and responses $y_i \in \mathbb{R}$. We fit a decision tree by partitioning training data using axis-aligned splits which maximize the decrease in impurity. Specifically, a split s at node \mathbf{v} partitions the data into two children nodes $\mathbf{v}_L = \{\mathbf{x}_i \in \mathbf{v} : x_{i,k} \leq \tau\}$ and $\mathbf{v}_R = \{\mathbf{x}_i \in \mathbf{v} : x_{i,k} > \tau\}$ for some covariate index k and threshold τ . We define the *impurity decrease* of s to be

$$\hat{\Delta}(s, \mathcal{D}) := N(\mathbf{v})^{-1} \left(\sum_{i: \mathbf{x}_i \in \mathbf{v}} (y_i - \bar{y}_{\mathbf{v}})^2 - \sum_{i: \mathbf{x}_i \in \mathbf{v}_L} (y_i - \bar{y}_{\mathbf{v}_L})^2 - \sum_{i: \mathbf{x}_i \in \mathbf{v}_R} (y_i - \bar{y}_{\mathbf{v}_R})^2 \right), \quad (1)$$

where $N(\mathbf{v})$ denotes the number of samples in node \mathbf{v} and $\bar{y}_{\mathbf{v}}$ denotes the mean response in node \mathbf{v} .

For a tree with *structure* $\mathcal{S} = \{s_1, \dots, s_m\}$, the MDI of feature X_k is defined as

$$MDI_k(\mathcal{S}, \mathcal{D}) := \sum_{s \in \mathcal{S}^{(k)}} n^{-1} N(\mathbf{v}(s)) \hat{\Delta}(s, \mathcal{D}), \quad (2)$$

where $\mathcal{S}^{(k)}$ represents the splits which threshold feature X_k and $\mathbf{v}(s)$ is the node split by s .

3.2 Connecting MDI to R^2 Values from Linear Regression

Using the notation described above, we define the stump function

$$\psi(\mathbf{x}_i; s) = \frac{N(\mathbf{v}_R) \mathbf{1}\{x_{i,k} \leq \tau\} - N(\mathbf{v}_L) \mathbf{1}\{x_{i,k} > \tau\}}{\sqrt{N(\mathbf{v}_L) N(\mathbf{v}_R)}}. \quad (3)$$

Note that ψ takes three values, corresponding to whether the observation \mathbf{x} is below the threshold, above the threshold, or not contained in node \mathbf{v} . Concatenating the stump functions for all m splits in the tree with all observations in $\mathbf{X} \in \mathbb{R}^{n \times p}$ results in feature map $\Psi(\mathbf{X}; \mathcal{S}) := (\psi(\mathbf{X}; s_1), \dots, \psi(\mathbf{X}; s_m)) \in \mathbb{R}^{n \times m}$. Klusowski and Tian [32] showed that the fitted decision tree

model predictions are equivalent to those of the ordinary least squares (OLS) model achieved by regressing the responses \mathbf{y} on $\Psi(\mathbf{X}; \mathcal{S})$. Agarwal et al. [23] further build on this connection between decision trees and linear models by deriving a connection between MDI and R^2 , stated next.

Proposition 1 (Agarwal et al. [23]) *Assume a tree fit on bootstrapped dataset $\mathcal{D}^* = (\mathbf{X}^*, \mathbf{y}^*)$ has structure \mathcal{S} . Then, for feature X_k , we have:*

$$MDI_k(\mathcal{S}, \mathcal{D}^*) \propto R^2(\mathbf{y}, \hat{\mathbf{y}}^{(k)}), \quad (4)$$

where $\hat{\mathbf{y}}^{(k)} \in \mathbb{R}^n$ is the vector of predicted responses from the OLS regression $\mathbf{y}^* \sim \Psi(\mathbf{X}^*; \mathcal{S}^{(k)})$.

This relationship helps us better understand the following well-known drawbacks of MDI:

1. **Overfitting.** In a fixed regression design, the amount of overfitting is proportional to the degrees of freedom [33]. Thus, MDI is more overfit for features with a higher number splits.
2. **Bias against correlated and high-entropy features.** CART splits on high entropy and low correlation features, regardless of their association with the outcome [21, 22]. Thus, signal features which are highly correlated with noise receive less splits, resulting in lower MDI importance.
3. **Bias against additive models** The piecewise-constant axis-aligned splits of trees make them inefficient estimators of additive functions [34, 35], which are common in real-world data [36].

The MDI+ framework [23] for global feature importance mitigates these drawbacks through the use of out-of-bag (OOB) samples and regularized GLMs, but falls short of being able to explain individual predictions. See Appendix A for a detailed overview of MDI+.

3.3 The Local MDI+ Framework

We propose LMDI+, an extension of MDI+ to the sample-specific setting as follows.

1. **Obtain expanded representation.** Each tree in an RF is fit on a bootstrapped dataset $\mathcal{D}^* = (\mathbf{X}^*, \mathbf{y}^*)$. MDI regresses only on in-bag samples $\Psi(\mathbf{X}^*; \mathcal{S})$. LMDI+ instead appends the raw feature $\mathbf{x}_k \in \mathbb{R}^n$ to the feature map consisting of both in-bag and OOB samples, yielding the transformed representation $\tilde{\Psi}^{(k)}(\mathbf{X}) = \tilde{\Psi}(\mathbf{X}; \mathcal{S}^{(k)}) = [\Psi(\mathbf{X}; \mathcal{S}^{(k)}), \mathbf{x}_k]$.
2. **Fit regularized GLM.** Instead of using OLS, fit a regularized GLM \mathcal{G} with link function g and penalty λ by regressing response \mathbf{y} on the transformed data $\tilde{\Psi}(\mathbf{X}) = \tilde{\Psi}(\mathbf{X}; \mathcal{S})$.
3. **Calculate feature attributions.** Let $\hat{\beta}_\lambda^{(k)}$ represent the GLM coefficients corresponding to the features in $\tilde{\Psi}^{(k)}(\mathbf{X})$. For observation \mathbf{x} , we then define the LMDI+ of the k th feature to be $LMDI_k^+(\mathbf{x}, \mathcal{S}^{(k)}, \mathcal{G}) := \tilde{\Psi}^{(k)}(\mathbf{x})^\top \hat{\beta}_\lambda^{(k)}$ if $\mathcal{S}^{(k)} \neq \emptyset$, and zero otherwise.

After computing $LMDI_k^+(\mathbf{x}, \mathcal{S}^{(k)}, \mathcal{G})$ for $k = 1, \dots, p$, we rank features by the absolute value of their importance. The LMDI+ scores of an ensemble are obtained by averaging the scores of its trees.

We now describe how each of the above steps helps mitigate the biases described in Section 3.2.

1. **Tackling overfitting.** Regularized GLMs limit the degrees of freedom by penalizing excess splits. Additionally, using OOB samples allows for better generalization by ensuring MDI is not solely measured on the same in-bag data used to fit the tree.
2. **Tackling correlation bias.** Regularized GLMs penalize highly correlated features, helping correct for the implicit bias of trees which split on them more frequently.
3. **Tackling bias against additive models.** Appending the raw feature (and any transformations of it) to the data matrix adds continuous features that improve the estimation of additive functions.

Outline of results. The following sections present experiments evaluating the performance of LMDI+. Section 4 demonstrates LMDI+ effectively captures signal features across a wide range of settings. Section 5 shows that LMDI+ produces stable feature importance rankings across different random model initializations. Section 6 conducts an ablation study to assess the contribution of each component in the LMDI+ framework. Lastly, Section 7 and Section 8 describe how LMDI+ enhances two practical use cases for local feature importance.

In the results presented in Sections 4-8, we pick ElasticNet as the GLM due to its combination of ℓ_1 and ℓ_2 penalties. Additional implementation details are provided in Appendix B.

4 LMDI+ Better Captures Signal Features

In this section, we demonstrate that LMDI+ better differentiates between signal and non-signal features at the individual level across a variety of datasets and data-generating processes. We begin by introducing the datasets and baselines used in our evaluation.

Datasets. We selected commonly-used benchmarks datasets from the OpenML repository [37]. For regression tasks, we use datasets from the CTR23 curated tabular regression benchmark [38]. For classification tasks, we use datasets from Grinsztajn et al. [39]’s benchmark and the CC18 curated classification benchmark [40]. We selected six regression datasets and six classification datasets with a large number of features from the repository, consistently using these datasets across all experiments. Details of the selected datasets are provided in Appendix C.

Baselines. We compare LMDI+ to commonly-used LFI methods LIME and TreeSHAP to evaluate performance. We further include LMDI (Section 3.3) to highlight the improvements of our approach.

4.1 Data-Inspired Synthetic Experiments

Evaluating LFI methods is challenging due to the absence of ground-truth feature importances in real-world datasets. To overcome this, we begin by assessing each method’s ability to distinguish signal from non-signal features in synthetic settings where the true importance is known. To make these simulations more realistic, we use real-world covariates to capture naturally occurring correlation patterns and noise and generate responses via analytic functions.

Setup. In each simulation, a subset of features is randomly selected from each dataset described above to serve as signal features, which are then incorporated into the following response function.

1. Linear model: $\mathbb{E}[Y | X] = \sum_{m=1}^5 X_m$
2. Interaction model: $\mathbb{E}[Y | X] = \sum_{m=1}^3 X_{2m-1} X_{2m}$
3. Linear + locally-spiky-sparse (LSS): $\mathbb{E}[Y | X] = \sum_{m=1}^3 X_{2m-1} + \mathbb{1}(X_{2m-1} > 0) \mathbb{1}(X_{2m} > 0)$

Classification simulations then pass $\mathbb{E}[Y | X]$ through a logistic link function to generate binary responses. These response functions were selected to reflect real world data-generating processes. Linear and interaction models are widely studied models in the machine learning literature [41, 42], while the linear plus locally-spiky-sparse model is commonly observed in fields like genomics [43].

Parameters. We vary both the signal-to-noise ratio (SNR) and the sample size. For regression, we measure the SNR by proportion of variance explained ($PVE = \frac{\text{Var}(\mathbb{E}[Y | X])}{\text{Var}(Y)}$). We then take $PVE \in \{0.1, 0.2, 0.4, 0.8\}$. For classification, noise levels are adjusted by randomly flipping $\{0\%, 5\%, 10\%, 15\%\}$ of the labels. Sample sizes are varied over $\{150, 500, 1000\}$.

Evaluation. We evaluate the task based on how well each LFI method classifies signal features over non-signal features. We treat this as a classification problem, where signal features are labeled as 1 (positive class) and noise features as 0 (negative class). We compute the AUROC score between the LFI scores and the signal labels for each test sample. Higher AUROC across instances indicates better performance.

Results. Figure 1 presents the results on two benchmark datasets with sample size 1000. LMDI+ consistently achieves higher AUROC across different response functions and SNRs. LMDI+’s superior ability to distinguish signal from noise is consistent across different datasets and sample sizes. Complete results for all datasets and sample sizes are provided in Appendix D.

4.2 LMDI+ is Robust to Strong Correlation

Existing LFI methods struggle to identify signal features when they are highly correlated with noisy ones. In this section, we show that LMDI+ is robust to strong correlation.

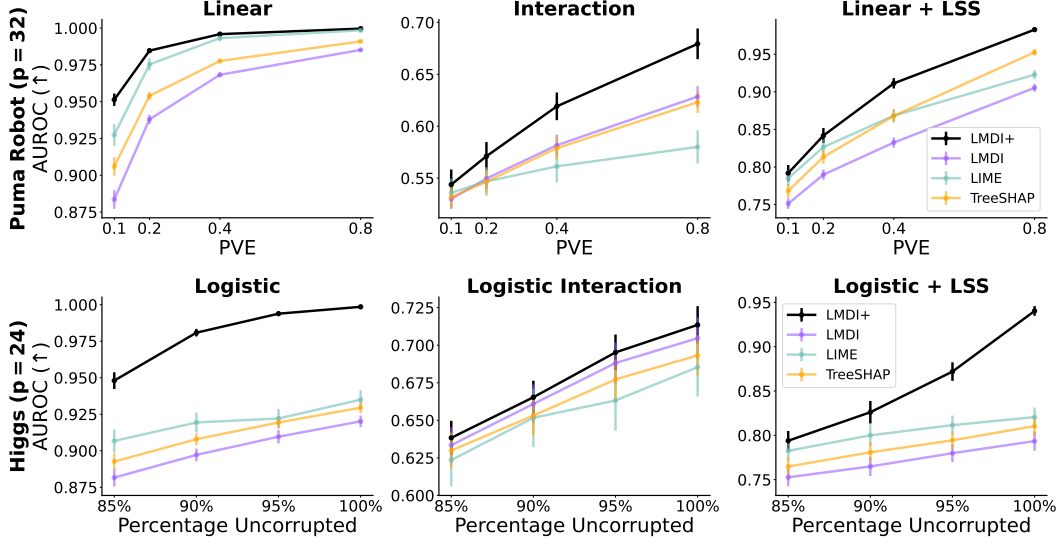


Figure 1: LMDI+ consistently achieves higher AUROC across different datasets, response functions and SNRs, demonstrating its superior ability to distinguish signal features from non-signal features. Results are averaged over 30 runs, error bars show the standard error of the mean.

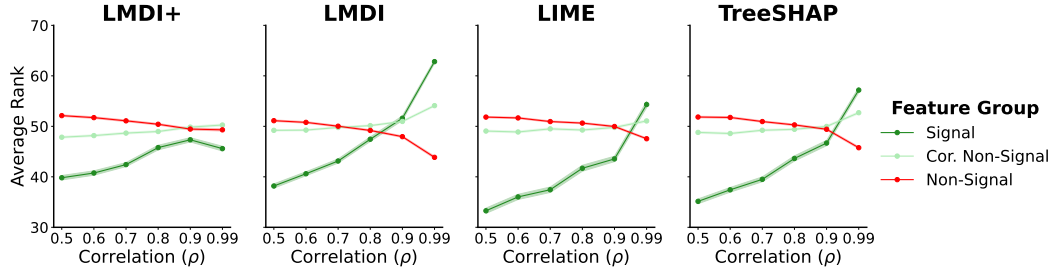


Figure 2: We show the average per sample ranks (± 1 SE) of each feature group under various levels of correlation ρ . In the presence of extreme correlation, only LMDI+ continues to rank the signal features as most important. Results are averaged over 50 runs.

Setup. We draw 250 samples $\mathbf{x} \sim \mathcal{N}_{100}(\mathbf{0}, \Sigma)$, where Σ has a block structure: features X_1, \dots, X_{50} share pairwise correlation ρ , while X_{51}, \dots, X_{100} are independent of all other features. Responses y are generated using the linear+LSS model from Section 4.1, which has signal features X_1, \dots, X_6 .

Parameters. We fix $PVE = 0.1$ and vary correlation $\rho \in \{0.5, 0.6, 0.7, 0.8, 0.9, 0.99\}$.

Evaluation. We divide the features into three groups: (1) signal features, (2) non-signal features that are correlated with signal, and (3) independent non-signal features. For each LFI method, we compute the average feature ranking of each group. Robust methods should consistently rank signal features above both types of non-signal features, regardless of correlation strength.

Results. Figure 2 displays the average per sample rank of each feature group according to various LFI methods. We observe that LMDI, LIME, and TreeSHAP all rank uncorrelated non-signal features above signal features in the presence of strong correlation. However, the use of regularized GLMs and OOB samples helps LMDI+ rank signal features as the most important across all levels of correlation.

4.3 Real Data Experiments

We now turn to evaluation using the real datasets described in Table 4. Since ground truth is unavailable, we adopt a commonly used remove-and-retrain evaluation technique [44, 45] to demonstrate that LMDI+ identifies features that are more predictive of the response.

Setup. For each observation, we kept only the top $k\%$ of features according to individual LFI rankings. All other features were replaced with their average. An RF model was then retrained on this masked training set and evaluated on the original test set. For computational efficiency, datasets with more than 2,000 samples were downsampled to 2,000.

Parameters. We vary the proportion of features retained per sample by selecting the top $k \in \{10\%, 20\%, \dots, 100\%\}$ of features, based on individual feature importance rankings.

Evaluation. A better LFI method should identify more predictive features and therefore achieve higher performance after retraining. For regression tasks, we report R^2 after retraining, and for classification tasks, we report AUROC.

Results. Figure 3 shows performance on the *Puma Robot* and *SARCOS* datasets (regression) and the *Higgs* and *Ozone* datasets (classification). LMDI+ achieves higher R^2 and AUROC after retraining on the masked data, demonstrating its ability to identify more predictive features. The performance gap between LMDI+ and the base-lines becomes even more pronounced when a smaller proportion of features is retained. We summarize the full results across all 12 datasets in Table 1, reporting the average rank of each method. LMDI+ consistently achieves the top rank across different feature selection levels. Results for all datasets are provided in Appendix E.

Method	Average Rank (\downarrow)			
	Top Features Retained			
	10%	20%	30%	40%
LMDI+	1.33	1.17	1.00	1.08
LMDI	3.25	2.92	2.92	2.92
LIME	2.33	2.50	2.67	2.50
TreeSHAP	3.08	3.42	3.42	3.50

Table 1: We report the average rank of methods across 12 datasets, where lower ranks (closer to 1) indicate better performance. LMDI+ consistently achieves the best rank across all feature proportions, identifying more predictive features. Results are averaged over 20 runs per dataset.

5 LMDI+ Produces More Stable Feature Importance Rankings

In this section, we show LMDI+ consistently produces more stable local feature importance rankings across different model initializations, addressing the instability of existing methods [17, 19, 46].

Setup. For each dataset described in Table 4, we trained five RFs models, each initialized with a different random seed. For each sample, we identified the top $k\%$ most important features according to each LFI method and counted the number of unique features selected across the five fitted models.

Parameters. We vary the proportion of features retained per sample by selecting the top $k \in \{10\%, 20\%, \dots, 100\%\}$ based on individual feature importance rankings. In addition, we vary the sample size by subsampling $\{150, 500, 1000\}$ instances from each dataset.

Evaluation. We measure the number of unique features selected for each instance across the five RFs fits, normalized by the total number of features. We report the average across all samples, with lower values indicating more stable and robust feature rankings.

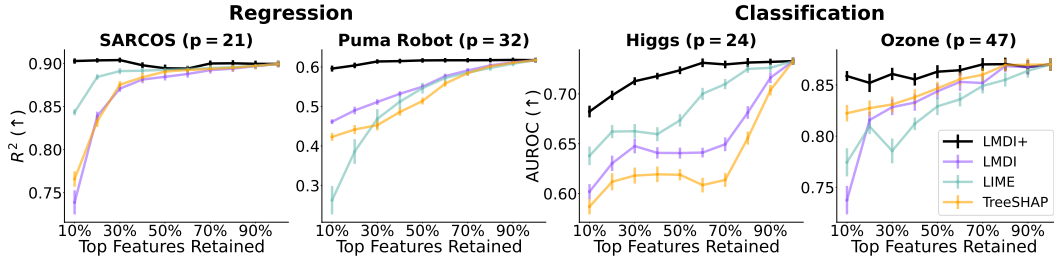


Figure 3: LMDI+ achieves higher R^2 and AUROC after retraining on masked training data, demonstrating its superior ability to identify signal features. Results are averaged over 20 runs.

Method	Average Rank (\downarrow)			
	Percent of Features Retained			
	Feature Selection		Stability	
	10%	20%	10%	20%
LMDI	2.33	1.92	2.75	2.67
LMDI with OOB samples	1.67	1.75	2.18	1.73
LMDI with OOB samples & raw features	1.67	1.17	1.17	1.08
LMDI+ (LMDI with OOB samples, raw features, & GLM)	1.25	1.17	1.17	1.00

Table 2: Ablation study for LMDI+ on real data experiments. Results show the rank between the specified method, TreeSHAP and LIME, where lower average rank indicates better performance.

Results. We present the results for *Puma Robot* and *SARCOS* datasets (regression) and the *Higgs* and *Ozone* datasets (classification) in Figure 4. Across varying sample sizes and percentages of selected features, LMDI+ consistently identifies the smallest number of unique features, indicating greater stability compared to the baselines. The complete results for all datasets are provided in Appendix F.

6 Ablation Analysis

As described in Section 3.3, our method builds upon LMDI by incorporating out-of-bag (OOB) samples, transformed features, and generalized linear models (GLMs). In this section, we conduct an ablation analysis to evaluate the contribution of each of these components.

We report results from real data feature selection experiments (Section 4.3) and stability experiments (Section 5), illustrating how each component helps address the known limitations of the baseline methods [16–20].

Table 2 summarizes the performance of different LMDI+ variants. We report the average rank across all 12 datasets, where a lower rank (closer to 1) indicates better performance. The ablation study reveals a clear performance improvement as more components are added, with the best results achieved when all components are included.

7 LMDI+ Finds Better Counterfactuals

Counterfactual explanations describe how an observation would need to change to obtain a different classification. They are typically computed on the observed data and thus treat all features equally, regardless of importance [47]. In Appendix G we show that using LFI to find counterfactuals yields explanations that prioritize proximity with respect to signal features. In this section, we demonstrate that using LMDI+ produces improved counterfactual explanations by preferring predictive features.

Setup. For each classification dataset in Table 4, we train an RF and compute LFI on both the training and test data. Counterfactuals are traditionally computed by finding the minimum-norm vector that crosses the decision boundary [48, 49]. However, this can lead to impossible feature values. To avoid

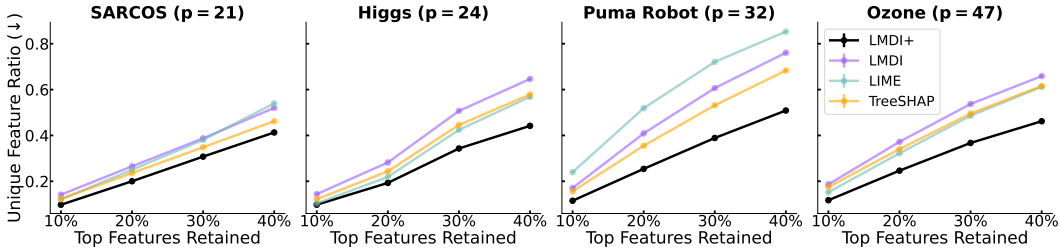


Figure 4: LMDI+ identifies a consistent set of influential features across distinct RF fits. The trend is more pronounced for datasets with a larger number of features. Results are averaged over 15 runs.

	Mean ℓ_1 Distance to Counterfactual (\downarrow)					
	House 16H	Higgs	Pol	Ozone	Jannis	Spam
LMDI+	7.8	18.1	9.0	33.9	40.8	15.3
LMDI	10.3	19.9	9.9	40.3	44.4	19.3
LIME	9.4	19.8	11.3	36.8	44.7	21.3
TreeSHAP	10.1	20.0	10.3	41.7	44.8	16.5

Table 3: LMDI+ detects closer counterfactual explanations than LIME and TreeSHAP.

such issues, we instead match the observation to the most similar training example using a kNN approach [50–52]. Specifically, for each test sample \mathbf{x} with predicted label \hat{y} and feature importance vector \mathbf{w} , we find the training sample \mathbf{x}_j which minimizes $\|\mathbf{w} - \mathbf{w}_j\|_1$ subject to $\hat{y} \neq \hat{y}_j$.

Evaluation. Good counterfactuals aim to be as similar as possible to the original observation, thus minimizing unnecessary changes. To measure similarity, we use the ℓ_1 distance (as suggested by Wachter et al. [48]) $\|\mathbf{x} - \mathbf{x}_j\|_1$ between the counterfactual and the test sample.

Results. Table 3 shows the mean ℓ_1 distance to the counterfactuals detected by each LFI method. We observe that for every dataset, LMDI+ has the smallest average distance, thus minimizing the amount of change necessary to flip the predictions.

8 Case Study: LMDI+ Discovers More Homogeneous Subgroups

Subgroup identification allows practitioners to better understand patterns which exist in their data. Particularly, clustering algorithms partition observations into subgroups which may share common traits. In this section, we investigate how using LFI scores to form homogeneous subgroups can simplify the underlying prediction task.

Setup. We select ‘Miami Housing’ from the benchmarks listed in Table 4 due to its easily understandable task (predict sale price) and features (location, size, etc.). Using a 50/50 train-test split, we fit an RF on the training data and calculate LFI scores on the test data. We then partition the data into subgroups by performing k -means clustering (for $k = 2, \dots, 10$) on each method’s LFI matrix.

Evaluation. We fit an OLS regression on each subgroup detected by an LFI method. If the LFI method has discovered more homogeneous subgroups, the simple OLS models should perform better. We examine the mean squared error of the regression models across $k = 2, \dots, 10$ for each method.

Results. Figure 5 displays how subgroup selection changes the error of sale price prediction. The constant ‘Global’ line represents the error of OLS fit to the entire dataset. We observe that clustering on LFI scores achieves lower error than fitting a model on the full data. Among LFI methods, LMDI+ consistently yields the lowest error. Furthermore, the MSE from the clusters generated by LMDI+ continues to decrease as k increases, whereas TreeSHAP’s clusters see a slight increase for large k . Appendix H details an exploration of the subgroups formed by clustering on LMDI+ scores.

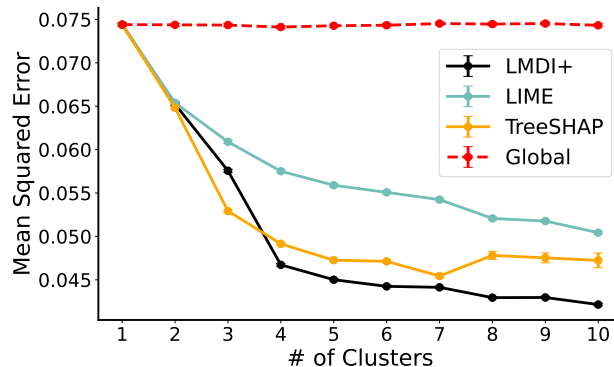


Figure 5: We show the MSE ($\pm 1SE$) of linear regressions fit on each cluster. We observe a steep drop until $k = 4$, after which MSE levels off. LMDI+ outperforms LIME and TreeSHAP, reducing error by 40% over the ‘Global’ model.

9 Discussion

LMDI+ extends MDI+ to the sample-specific setting. LMDI+ not only outperforms other LFI methods in identifying signal features, but displays the highest stability. This makes LMDI+ particularly valuable in high-stakes applications where trustworthy local explanations are critical. Further, we show how LMDI+ can be used for counterfactual explanations and subgroup discovery.

Future Work. LMDI+ offers many opportunities for future extensions. While currently demonstrated with random forests, it can be applied to any tree-based algorithm, including popular gradient-based methods like XGBoost. Its flexible framework also supports various choices of generalized linear models and transformations for continuous features. Future work could also include characterizing the impact of interactions as well as exploring the use of deep learning models instead of GLMs.

Limitations. LMDI+ can only be applied to tree-based methods due to its reliance on the specific model structure. Furthermore, due to the recursive splitting within a tree, the computational complexity of LMDI+ grows exponentially with the tree’s depth. However, we note that calculating the GLM coefficients for LMDI+ is a one-time cost, allowing LMDI+ to be efficiently applied to future observations by simply taking the product of the fitted coefficients and the transformed features.

Acknowledgments and Disclosure of Funding

ZTR is supported by the National Science Foundation Graduate Research Fellowship Program under Grant No. DGE-2146752. Any opinions, findings, and conclusions or recommendations expressed in this material are those of the authors and do not necessarily reflect the views of the National Science Foundation.

BY acknowledges partial support from NSF grant DMS-2413265, NSF grant DMS 2209975, NSF grant 2023505 on Collaborative Research: Foundations of Data Science Institute (FODSI), the NSF and the Simons Foundation for the Collaboration on the Theoretical Foundations of Deep Learning through awards DMS-2031883 and 814639, NSF grant MC2378 to the Institute for Artificial CyberThreat Intelligence and Operation (ACTION), and NIH grant R01GM152718.

References

- [1] Chandan Singh, Keyan Nasser, Yan Shuo Tan, Tiffany Tang, and Bin Yu. imodels: a python package for fitting interpretable models. *Journal of Open Source Software*, 6(61):3192, 2021.
- [2] Leo Breiman. Random forests. *Machine Learning*, 45(1):5–32, 2001.
- [3] Yoav Freund and Robert E. Schapire. A decision-theoretic generalization of on-line learning and an application to boosting. In Paul Vitányi, editor, *Computational Learning Theory*, pages 23–37, Berlin, Heidelberg, 1995. Springer Berlin Heidelberg. ISBN 978-3-540-49195-8.
- [4] Ravid Shwartz-Ziv and Amitai Armon. Tabular data: Deep learning is not all you need. *Information Fusion*, 81:84–90, 2022.
- [5] Yury Gorishniy, Ivan Rubachev, Valentin Khrulkov, and Artem Babenko. Revisiting deep learning models for tabular data. *Advances in neural information processing systems*, 34: 18932–18943, 2021.
- [6] G. Haripriya, K. Abinaya, N. Aarth, and P. Praveen Kumar. Random forest algorithms in health care sectors: a review of applications. *International Journal of Recent Development in Computer Technology & Software Application*, 2021.
- [7] Zhongyuan Liang, Arvind Suresh, and Irene Y Chen. Treatment non-adherence bias in clinical machine learning: A real-world study on hypertension medication. *arXiv preprint arXiv:2502.19625*, 2025.
- [8] Bette Loef, Albert Wong, Nicole AH Janssen, Maciek Strak, Jurriaan Hoekstra, H Susan J Picavet, HC Hendrick Boshuizen, WM Monique Verschuren, and Gerrie-Cor M Herber. Using random forest to identify longitudinal predictors of health in a 30-year cohort study. *Scientific Reports*, 12(1):10372, 2022.
- [9] Nikolaj Tollenaar and Peter GM Van Der Heijden. Optimizing predictive performance of criminal recidivism models using registration data with binary and survival outcomes. *PloS one*, 14(3):e0213245, 2019.
- [10] Abdulrahman Alsubayhin, Muhammad Sher Ramzan, and Bander Alzahrani. Crime prediction model using three classification techniques: Random forest, logistic regression, and lightgbm. *International Journal of Advanced Computer Science & Applications*, 15(1), 2024.
- [11] Olha Kovalchuk, Mikolaj Karpinski, Serhiy Banakh, Mykhailo Kasianchuk, Ruslan Shevchuk, and Nataliya Zagorodna. Prediction machine learning models on propensity convicts to criminal recidivism. *Information*, 14(3):161, 2023.
- [12] Marco Tulio Ribeiro, Sameer Singh, and Carlos Guestrin. "why should i trust you?": Explaining the predictions of any classifier, 2016. URL <https://arxiv.org/abs/1602.04938>.
- [13] Scott Lundberg and Su-In Lee. A unified approach to interpreting model predictions, 2017. URL <https://arxiv.org/abs/1705.07874>.

- [14] Songchang Shi, Xiaobin Pan, Lihui Zhang, Xincan Wang, Yingfeng Zhuang, Xingsheng Lin, Songjing Shi, Jianzhang Zheng, and Wei Lin. An application based on bioinformatics and machine learning for risk prediction of sepsis at first clinical presentation using transcriptomic data. *Frontiers in Genetics*, 13:979529, 2022.
- [15] Viswan Vimbi, Noushath Shaffi, and Mufti Mahmud. Interpreting artificial intelligence models: a systematic review on the application of lime and shap in alzheimer’s disease detection. *Brain Informatics*, 11(1):10, 2024.
- [16] Blair Bilodeau, Natasha Jaques, Pang Wei Koh, and Been Kim. Impossibility theorems for feature attribution. *Proceedings of the National Academy of Sciences*, 121(2):e2304406120, 2024. doi: 10.1073/pnas.2304406120. URL <https://www.pnas.org/doi/abs/10.1073/pnas.2304406120>.
- [17] Muhammad Rehman Zafar and Naimul Mefraz Khan. Dlime: A deterministic local interpretable model-agnostic explanations approach for computer-aided diagnosis systems. *arXiv preprint arXiv:1906.10263*, 2019.
- [18] Xuanxiang Huang and Joao Marques-Silva. On the failings of shapley values for explainability. *International Journal of Approximate Reasoning*, 171:109112, 2024. ISSN 0888-613X. doi: <https://doi.org/10.1016/j.ijar.2023.109112>. URL <https://www.sciencedirect.com/science/article/pii/S0888613X23002438>. Synergies between Machine Learning and Reasoning.
- [19] Yujia Zhang, Kuangyan Song, Yiming Sun, Sarah Tan, and Madeleine Udell. " why should you trust my explanation?" understanding uncertainty in lime explanations. *arXiv preprint arXiv:1904.12991*, 2019.
- [20] David Alvarez-Melis and Tommi S Jaakkola. On the robustness of interpretability methods. *arXiv preprint arXiv:1806.08049*, 2018.
- [21] Carolin Strobl, Anne-Laure Boulesteix, Achim Zeileis, and Torsten Hothorn. Bias in random forest variable importance measures: Illustrations, sources and a solution. *BMC Bioinformatics*, 8(1):25, Jan 2007. ISSN 1471-2105. doi: 10.1186/1471-2105-8-25. URL <https://doi.org/10.1186/1471-2105-8-25>.
- [22] Robin Genuer, Jean-Michel Poggi, and Christine Tuleau-Malot. Variable selection using random forests. *Pattern Recognition Letters*, 31(14):2225–2236, 2010. ISSN 0167-8655. doi: <https://doi.org/10.1016/j.patrec.2010.03.014>. URL <https://www.sciencedirect.com/science/article/pii/S0167865510000954>.
- [23] Abhineet Agarwal, Ana M Kenney, Yan Shuo Tan, Tiffany M Tang, and Bin Yu. Mdi+: A flexible random forest-based feature importance framework. *arXiv preprint arXiv:2307.01932*, 2023.
- [24] Guolin Ke, Qi Meng, Thomas Finley, Taifeng Wang, Wei Chen, Weidong Ma, Qiwei Ye, and Tie-Yan Liu. Lightgbm: A highly efficient gradient boosting decision tree. *Advances in neural information processing systems*, 30, 2017.
- [25] L. Breiman, J. Friedman, R.A. Olshen, and C.J. Stone. *Classification and Regression Trees*. Chapman and Hall/CRC, 1984.
- [26] Yan Shuo Tan, Chandan Singh, Keyan Nasser, Abhineet Agarwal, James Duncan, Omer Ronen, Matthew Epland, Aaron Kornblith, and Bin Yu. Fast interpretable greedy-tree sums. *Proceedings of the National Academy of Sciences*, 122(7):e2310151122, 2025.
- [27] J Ross Quinlan et al. Bagging, boosting, and c4. 5. In *Aaai/Iaai*, vol. 1, pages 725–730. Citeseer, 1996.
- [28] Mousumi Banerjee, Evan Reynolds, Hedvig B Andersson, and Brahmajee K Nallamothu. Tree-based analysis: a practical approach to create clinical decision-making tools. *Circulation: Cardiovascular Quality and Outcomes*, 12(5):e004879, 2019.

- [29] Susan Athey, Julie Tibshirani, and Stefan Wager. Generalized random forests. *The Annals of Statistics*, 47(2):1148 – 1178, 2019. doi: 10.1214/18-AOS1709. URL <https://doi.org/10.1214/18-AOS1709>.
- [30] Sumanta Basu, Karl Kumbier, James B Brown, and Bin Yu. Iterative random forests to discover predictive and stable high-order interactions. *Proceedings of the National Academy of Sciences*, 115(8):1943–1948, 2018.
- [31] Scott M. Lundberg, Gabriel Erion, Hugh Chen, et al. From local explanations to global understanding with explainable ai for trees. *Nature Machine Intelligence*, 2:56–67, Jan 2020. doi: 10.1038/s42256-019-0138-9. URL <https://doi.org/10.1038/s42256-019-0138-9>.
- [32] Jason M. Klusowski and Peter M. Tian. Large scale prediction with decision trees, 2023. URL <https://arxiv.org/abs/2104.13881>.
- [33] Trevor Hastie, Robert Tibshirani, Jerome H Friedman, and Jerome H Friedman. *The elements of statistical learning: data mining, inference, and prediction*, volume 2. Springer, 2009.
- [34] Yan Shuo Tan, Abhineet Agarwal, and Bin Yu. A cautionary tale on fitting decision trees to data from additive models: generalization lower bounds, 2021. URL <https://arxiv.org/abs/2110.09626>.
- [35] A. Tsybakov. Introduction to nonparametric estimation. In *Springer Series in Statistics*, 2008. URL <https://api.semanticscholar.org/CorpusID:42933599>.
- [36] Trevor Hastie and Robert Tibshirani. Generalized Additive Models. *Statistical Science*, 1(3):297 – 310, 1986. doi: 10.1214/ss/1177013604. URL <https://doi.org/10.1214/ss/1177013604>.
- [37] Joaquin Vanschoren, Jan N. van Rijn, Bernd Bischl, and Luis Torgo. Openml: Networked science in machine learning. *SIGKDD Explorations*, 15(2):49–60, 2013. doi: 10.1145/2641190.2641198. URL <http://doi.acm.org/10.1145/2641190.2641198>.
- [38] Sebastian Felix Fischer, Liana Harutyunyan Matthias Feurer, and Bernd Bischl. OpenML-CTR23 – a curated tabular regression benchmarking suite. In *AutoML Conference 2023 (Workshop)*, 2023. URL <https://openreview.net/forum?id=HebA0oMm94>.
- [39] Léo Grinsztajn, Edouard Oyallon, and Gaël Varoquaux. Why do tree-based models still outperform deep learning on tabular data?, 2022. URL <https://arxiv.org/abs/2207.08815>.
- [40] Bernd Bischl, Giuseppe Casalicchio, Matthias Feurer, Frank Hutter, Michel Lang, Rafael G. Mantovani, Jan N. van Rijn, and Joaquin Vanschoren. Openml benchmarking suites. *arXiv:1708.03731v2 [stat.ML]*, 2019.
- [41] Michael Tsang, James Enouen, and Yan Liu. Interpretable artificial intelligence through the lens of feature interaction. *arXiv preprint arXiv:2103.03103*, 2021.
- [42] Yunpeng Tai. A survey of regression algorithms and connections with deep learning. *arXiv preprint arXiv:2104.12647*, 2021.
- [43] Merle Behr, Yu Wang, Xiao Li, and Bin Yu. Provable boolean interaction recovery from tree ensemble obtained via random forests. *Proceedings of the National Academy of Sciences*, 119(22):e2118636119, 2022.
- [44] Nourah Alangari, Mohamed El Bachir Menai, Hassan Mathkour, and Ibrahim Almosallam. Exploring evaluation methods for interpretable machine learning: A survey. *Information*, 14(8): 469, 2023.
- [45] Sara Hooker, Dumitru Erhan, Pieter-Jan Kindermans, and Been Kim. A benchmark for interpretability methods in deep neural networks. *Advances in neural information processing systems*, 32, 2019.

- [46] Md Hasan. Understanding model predictions: A comparative analysis of shap and lime on various ml algorithms. *Journal of Scientific and Technological Research*, 5:17–26, 03 2024. doi: 10.59738/jstr.v5i1.23(17-26).eaqr5800.
- [47] Christoph Molnar. *Interpretable Machine Learning*. Leanpub, 3 edition, 2025. ISBN 978-3-911578-03-5. URL <https://christophm.github.io/interpretable-ml-book>.
- [48] Sandra Wachter, Brent Mittelstadt, and Chris Russell. Counterfactual explanations without opening the black box: Automated decisions and the gdpr. *Harv. JL & Tech.*, 31:841, 2017.
- [49] Susanne Dandl, Christoph Molnar, Martin Binder, and Bernd Bischl. Multi-objective counterfactual explanations. In *International conference on parallel problem solving from nature*, pages 448–469. Springer, 2020.
- [50] Evelyn Fix. *Discriminatory analysis: nonparametric discrimination, consistency properties*, volume 1. USAF school of Aviation Medicine, 1985.
- [51] Chhavi Yadav and Kamalika Chaudhuri. Behavior of k-nn as an instance-based explanation method. In *Joint European Conference on Machine Learning and Knowledge Discovery in Databases*, pages 90–96. Springer, 2021.
- [52] Dieter Brughmans, Pieter Leyman, and David Martens. Nice: an algorithm for nearest instance counterfactual explanations. *Data mining and knowledge discovery*, 38(5):2665–2703, 2024.
- [53] Asa Ben-Hur, Andre Elisseeff, and Isabelle Guyon. A stability based method for discovering structure in clustered data. In *Biocomputing 2002*, pages 6–17. World Scientific, 2001.

A The MDI+ Framework

MDI+ allows for a more flexible modeling framework, reducing the biases of MDI through additions such as out-of-bag samples and regularized GLMs. Particularly, MDI+ does the following:

1. **Obtain enhanced representation.** Each tree in an RF is fit on a bootstrapped dataset $\mathcal{D}^* = (\mathbf{X}^*, \mathbf{y}^*)$. MDI regresses only on in-bag samples $\Psi(\mathbf{X}^*; \mathcal{S})$. MDI+ instead appends the raw feature $\mathbf{x}_k \in \mathbb{R}^n$ to the feature map consisting of both in-bag and out-of-bag samples, yielding the transformed representation $\tilde{\Psi}^{(k)}(\mathbf{X}) = \tilde{\Psi}(\mathbf{X}; \mathcal{S}^{(k)}) = [\Psi(\mathbf{X}; \mathcal{S}^{(k)}), \mathbf{x}_k]$.
2. **Fit regularized GLM.** Instead of using OLS, fit a regularized GLM \mathcal{G} with link function g and penalty λ by regressing response \mathbf{y} on the transformed data $\tilde{\Psi}(\mathbf{X}) = \tilde{\Psi}(\mathbf{X}; \mathcal{S})$.
3. **Make partial model predictions.** Let $\tilde{\Psi}^{(j)}$ denote the vector of average values for features in $\tilde{\Psi}^{(j)}(\mathbf{X})$. For $k = 1, \dots, p$, we then define the partial model predictions for each sample \mathbf{x}_i to be

$$\hat{y}_i^{(k)} = g^{-1} \left(\left[\tilde{\Psi}^{(1)}, \dots, \tilde{\Psi}^{(k-1)}, \tilde{\Psi}^{(k)}(\mathbf{x}_i), \tilde{\Psi}^{(k+1)}, \dots, \tilde{\Psi}^{(p)} \right] \hat{\beta}_{-i, \lambda} + \alpha_\lambda \right), \quad (5)$$

where $\hat{\beta}_{-i, \lambda}$ is the LOO coefficient vector learned without sample \mathbf{x}_i .

4. **Evaluate predictions.** For some user-specified similarity metric m and $k = 1, \dots, p$, we define

$$MDI_k^+(\mathcal{S}, \mathcal{D}^*, \tilde{\Psi}, \mathcal{G}, m) := m(\mathbf{y}, \hat{\mathbf{y}}^{(k)}). \quad (6)$$

The resulting MDI+ scores are a p -vector denoting the importance of each feature to the trained tree-based model.

B Implementation Details Configuration for Random Forest and GLM

For regression tasks, we use a `RandomForestRegressor` with `n_estimators = 100`, `min_samples_leaf = 5`, and `max_features = 0.33`. For classification tasks, we use a `RandomForestClassifier` with `n_estimators = 100`, `min_samples_leaf = 1`, and `max_features = "sqrt"`.

For regression tasks, we use `ElasticNetCV` with `cv = 3` and `l1_ratio = [0.1, 0.5, 0.99]` as the GLM. For classification tasks, we use `LogisticRegressionCV` with `penalty = "elasticnet"`, `l1_ratios = [0.1, 0.5, 0.99]`, `solver = "saga"`, and `cv = 3` as the GLM.

C Dataset Details

We selected datasets commonly used in machine learning benchmarks from the OpenML repository [37]. We consistently used the six regression datasets and six classification datasets listed in Table 4 below. The *Geographic Origin of Music* dataset from the repository had many duplicate columns, so we removed duplicate columns to address redundancy. The *Ozone* dataset contained many highly correlated features, we therefore removed features with pairwise correlations greater than 0.95. Each dataset was split into training and testing sets. The experiments in Sections 4-6 allocate 67% of the data to the training set and 33% to the testing set. The experiments in Sections 7 and 8 require more test points and thus use a 50/50 split.

Table 4: Real-world datasets used in the paper: regression (top panel), classification (bottom panel).

	Name	Task ID	Features
Regression	Miami Housing	361260	15
	SARCOS	361254	21
	Puma Robot	361259	32
	Wave Energy	361253	48
	Geographic Origin of Music	361243	72
	Super Conductivity	361242	81
Classification	House 16H	361063	16
	Higgs	361069	24
	Pol	361062	26
	Ozone	9978	47
	Jannis	361071	54
	Spam	43	57

D Semi-Synthetic Feature Ranking Experiments

Here we present the results of all semi-synthetic feature ranking experiments for all datasets.

D.1 Linear Response Function

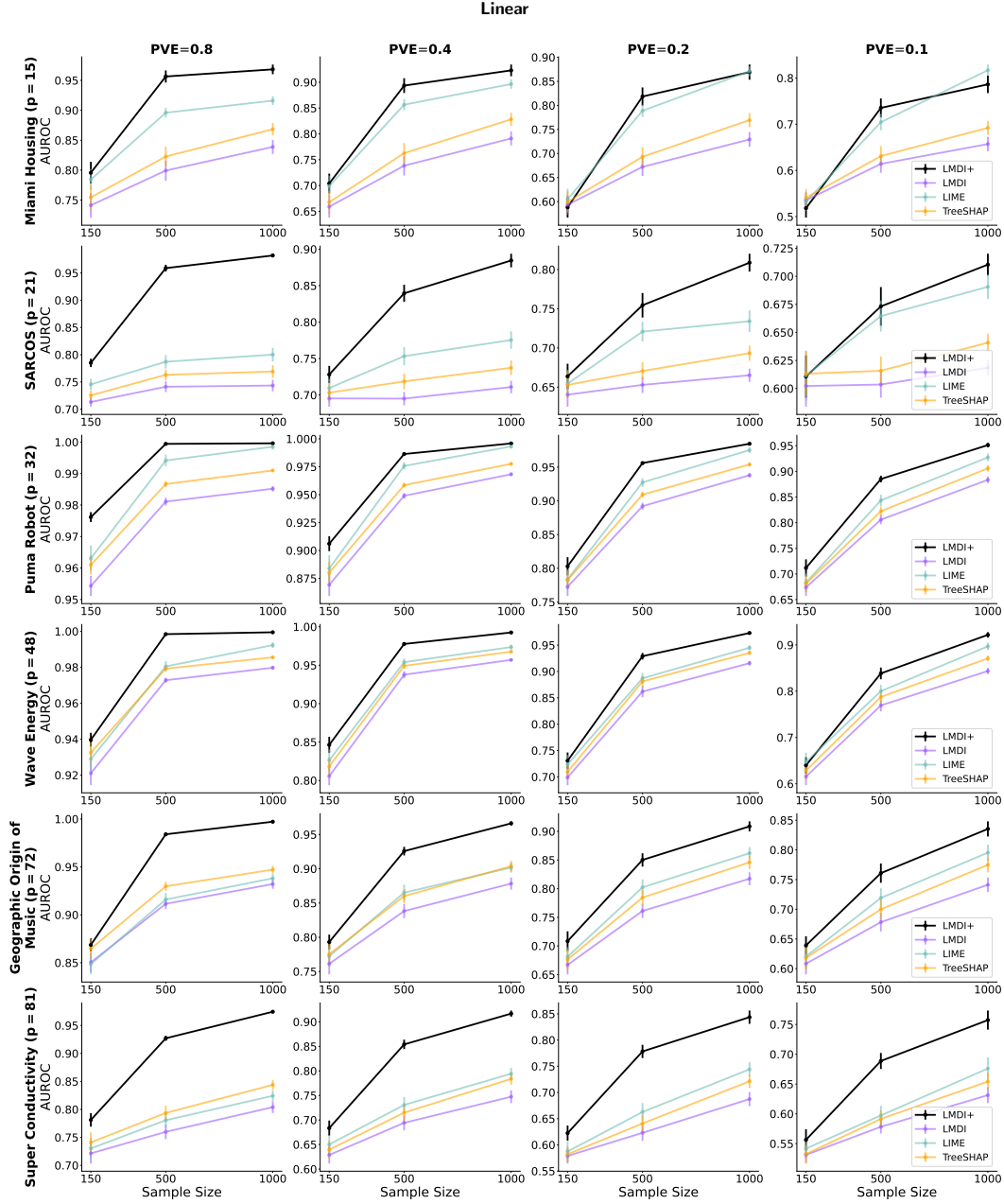


Figure 6: Across different sample sizes and signal-to-noise ratios in linear response function, LMDI+ demonstrates superior ability to distinguish signal features from non-signal features compared to other methods, with consistent trends observed across six regression datasets. Performance is reported as the average AUROC on test set samples and is averaged over 30 runs with different random sampling and the selection of signal features. Error bars show the standard error of the mean.

D.2 Interaction Response Function

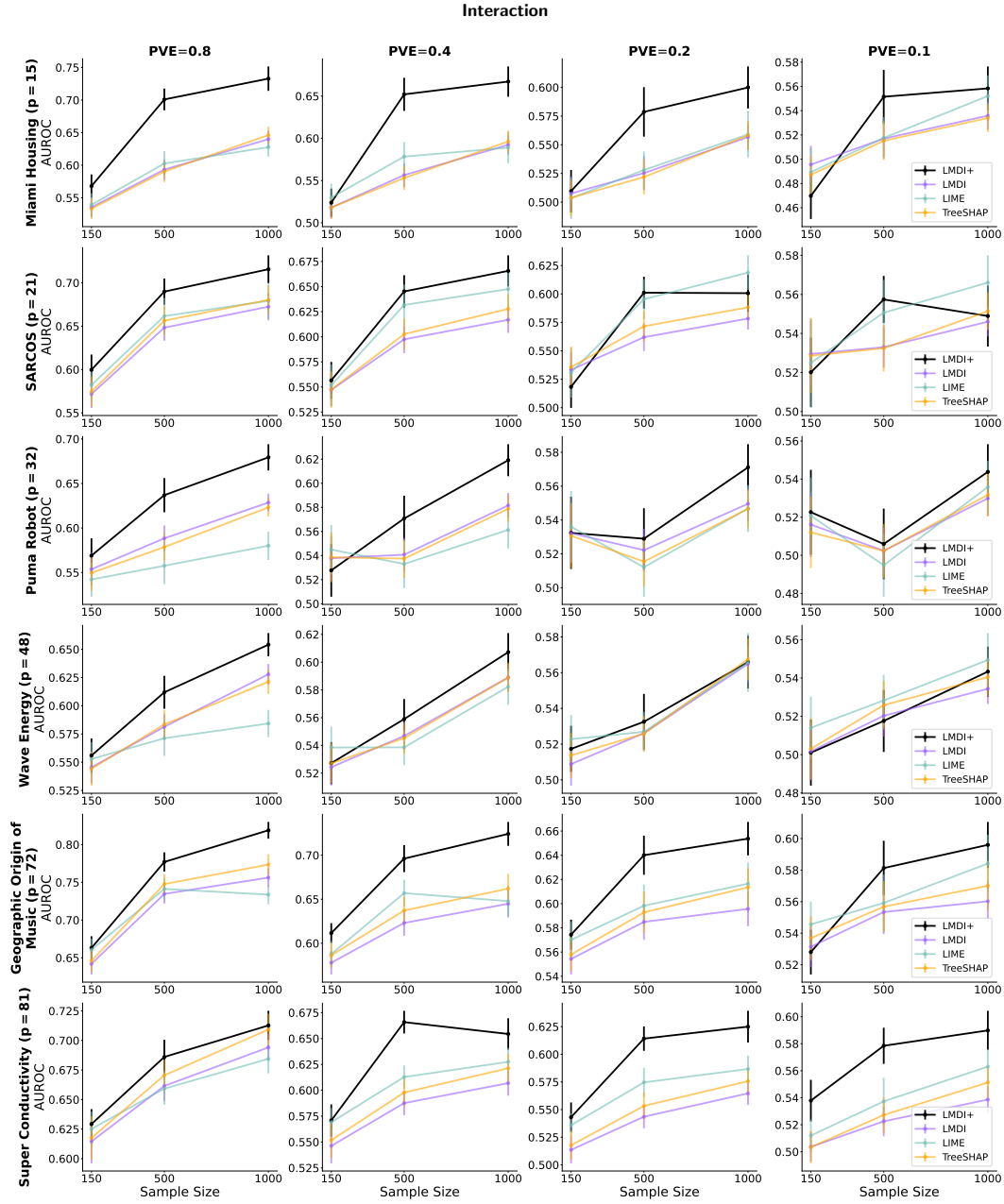


Figure 7: Across different sample sizes and signal-to-noise ratios in interaction response function, LMDI+ demonstrates superior ability to distinguish signal features from non-signal features compared to other methods, with consistent trends observed across six regression datasets. Performance is reported as the average AUROC on test set samples and is averaged over 30 runs with different random sampling and the selection of signal features. Error bars show the standard error of the mean.

D.3 Linear + LSS Response Function

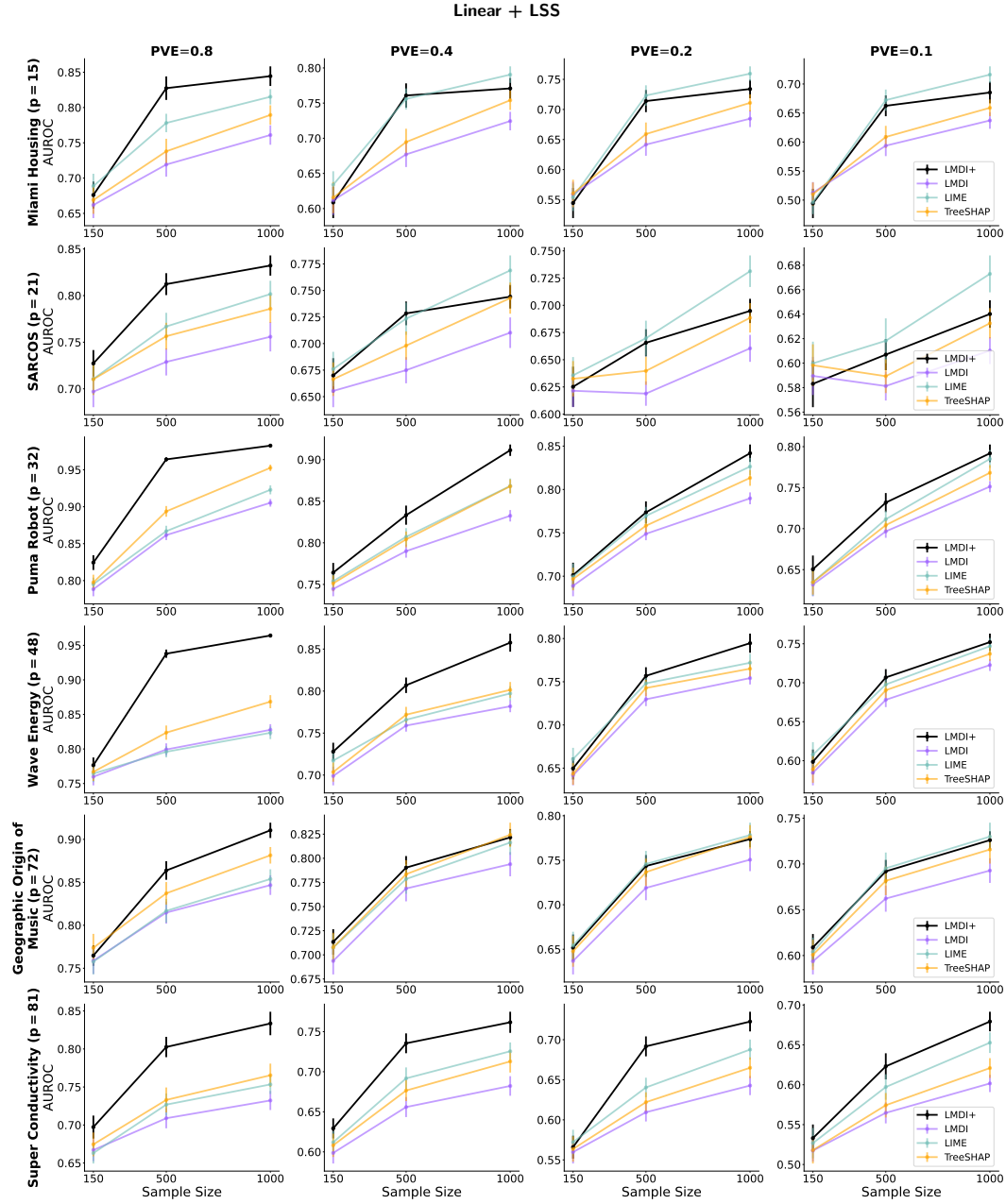


Figure 8: Across different sample sizes and signal-to-noise ratios in linear + LSS response function, LMDI+ demonstrates superior ability to distinguish signal features from non-signal features compared to other methods, with consistent trends observed across six regression datasets. Performance is reported as the average AUROC on test set samples and is averaged over 30 runs with different random sampling and the selection of signal features. Error bars show the standard error of the mean.

D.4 Logistic Linear Response Function

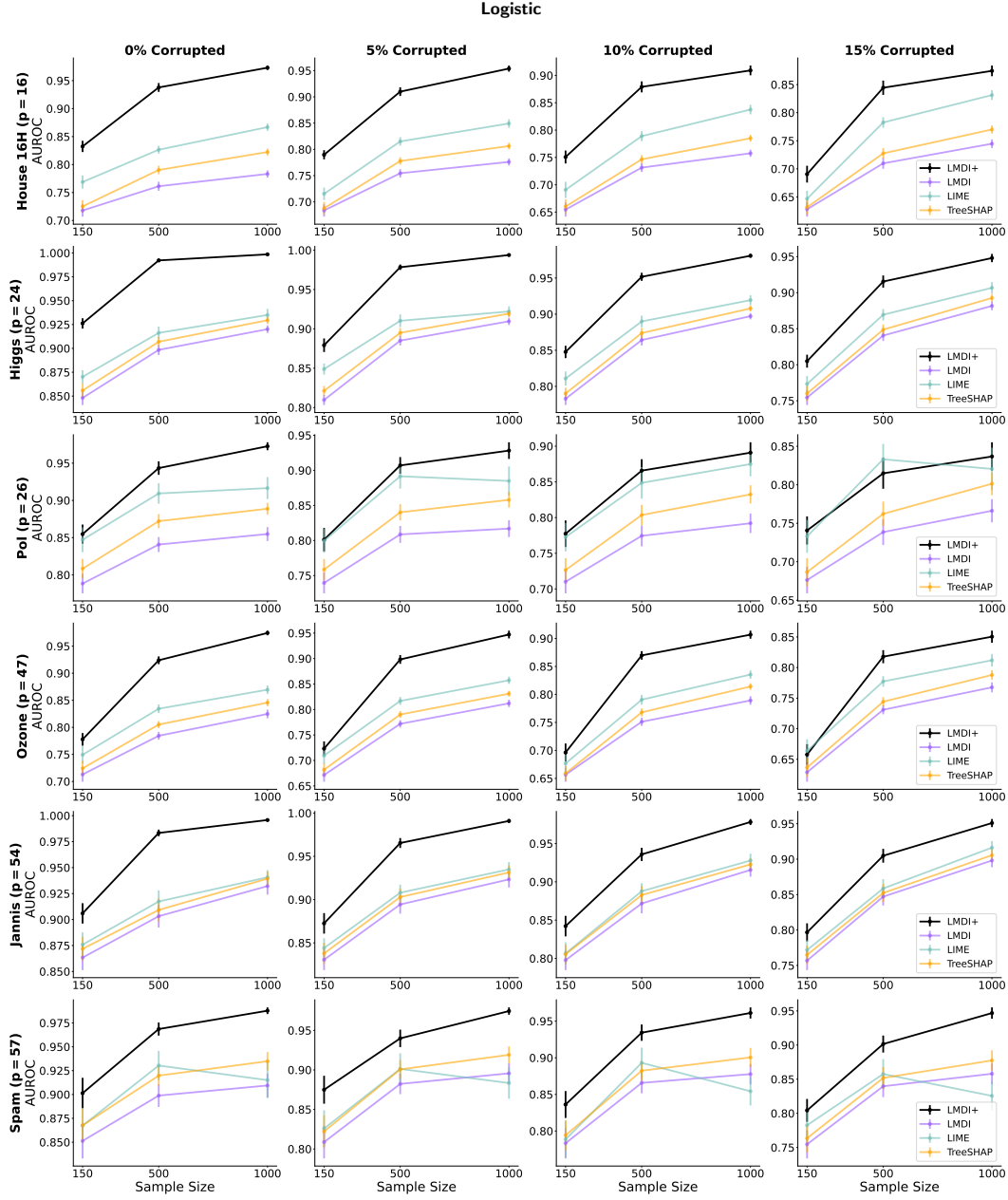


Figure 9: Across different sample sizes and signal-to-noise ratios in logistic response function, LMDI+ demonstrates superior ability to distinguish signal features from non-signal features compared to other methods, with consistent trends observed across six classification datasets. Performance is reported as the average AUROC on test set samples and is averaged over 30 runs with different random sampling and the selection of signal features. Error bars show the standard error of the mean.

D.5 Logistic Interaction Response Function

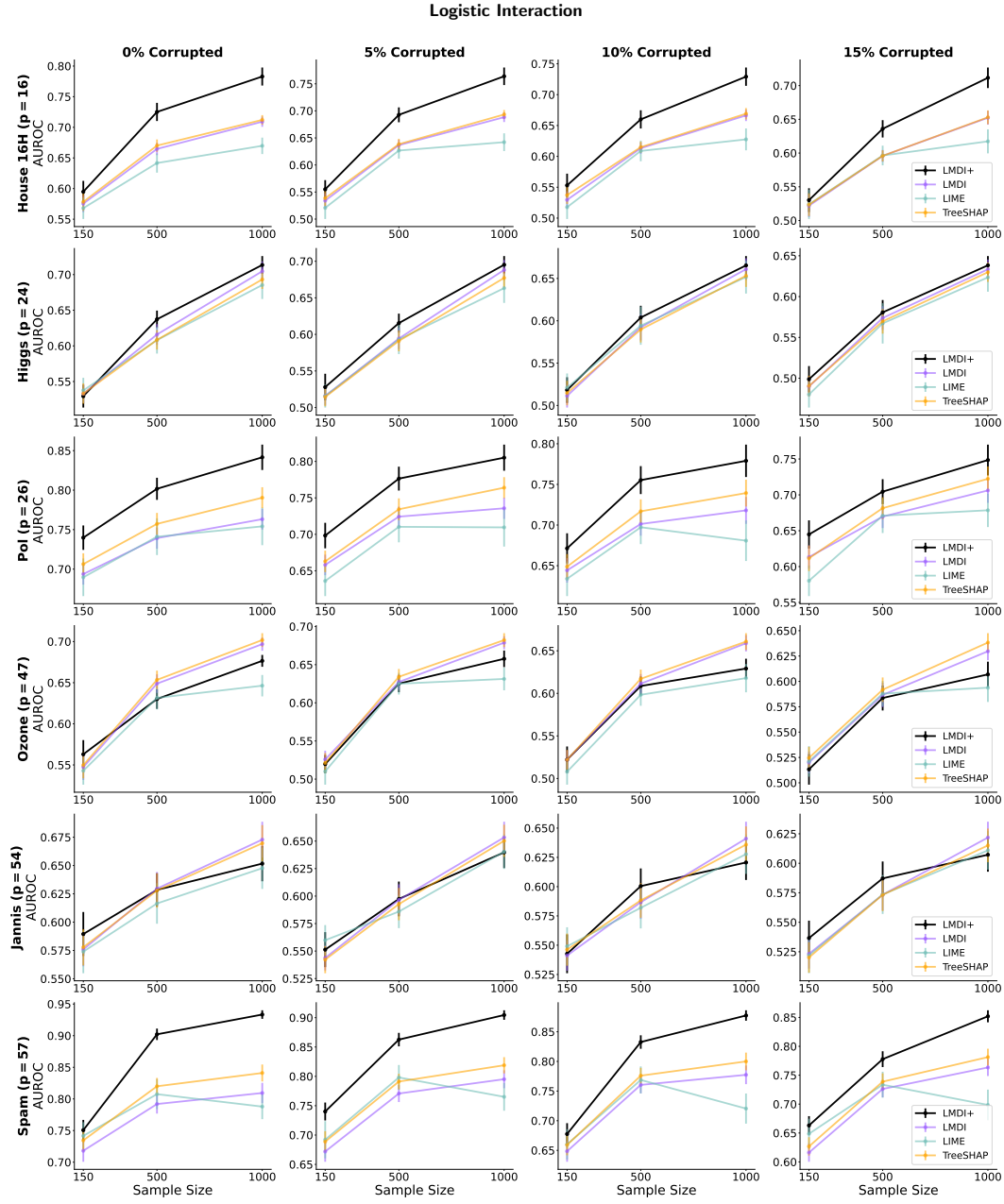


Figure 10: Across different sample sizes and signal-to-noise ratios in logistic interaction response function, LMDI+ demonstrates superior ability to distinguish signal features from non-signal features compared to other methods, with consistent trends observed across six classification datasets. Performance is reported as the average AUROC on test set samples and is averaged over 30 runs with different random sampling and the selection of signal features. Error bars show the standard error of the mean.

D.6 Logistic Linear + LSS Response Function

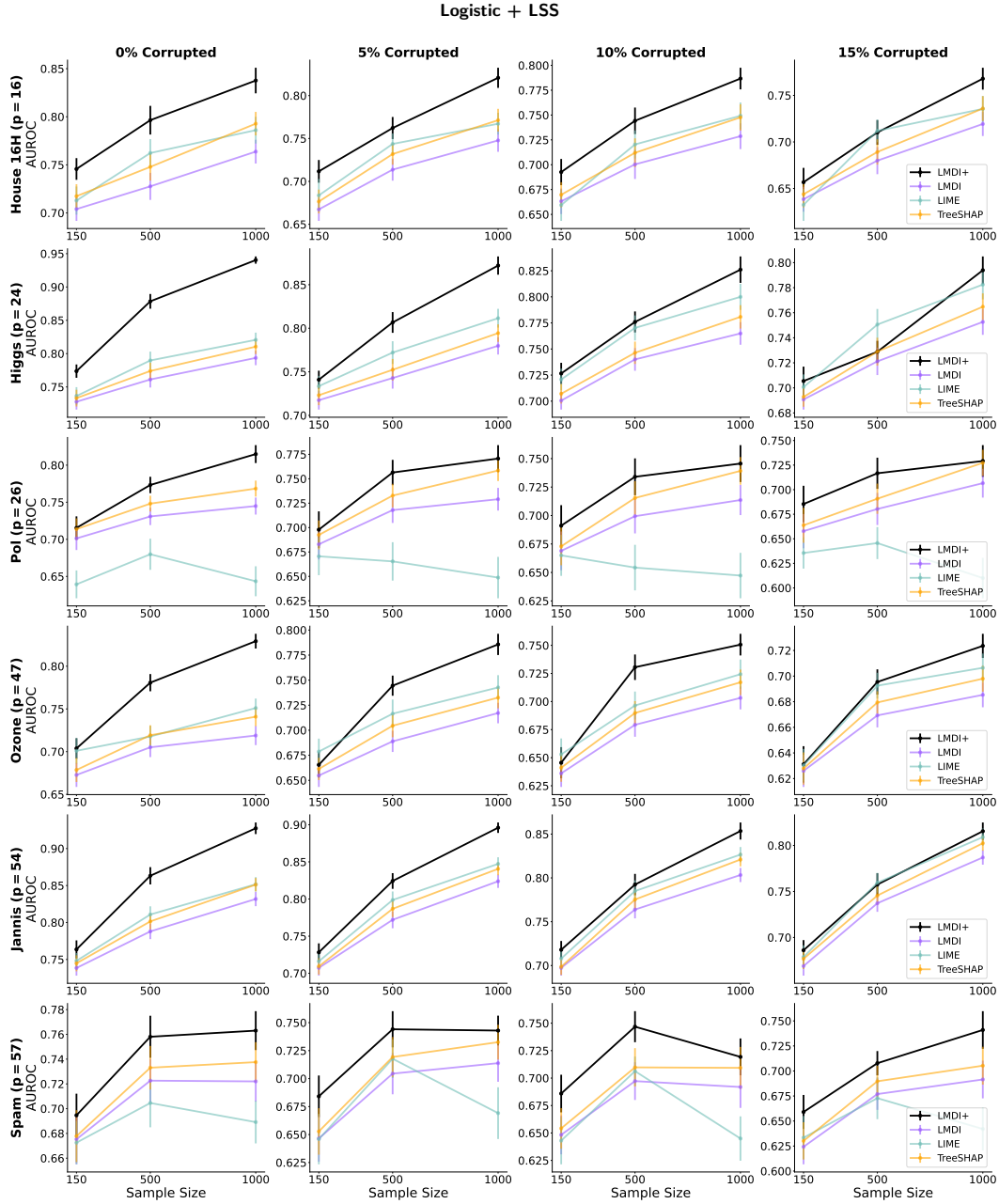


Figure 11: Across different sample sizes and signal-to-noise ratios in logistic linear + LSS response function, LMDI+ demonstrates superior ability to distinguish signal features from non-signal features compared to other methods, with consistent trends observed across six classification datasets. Performance is reported as the average AUROC on test set samples and is averaged over 30 runs with different random sampling and the selection of signal features. Error bars show the standard error of the mean.

E Real Data Experiments Results

E.1 Experiments Results on Full Data

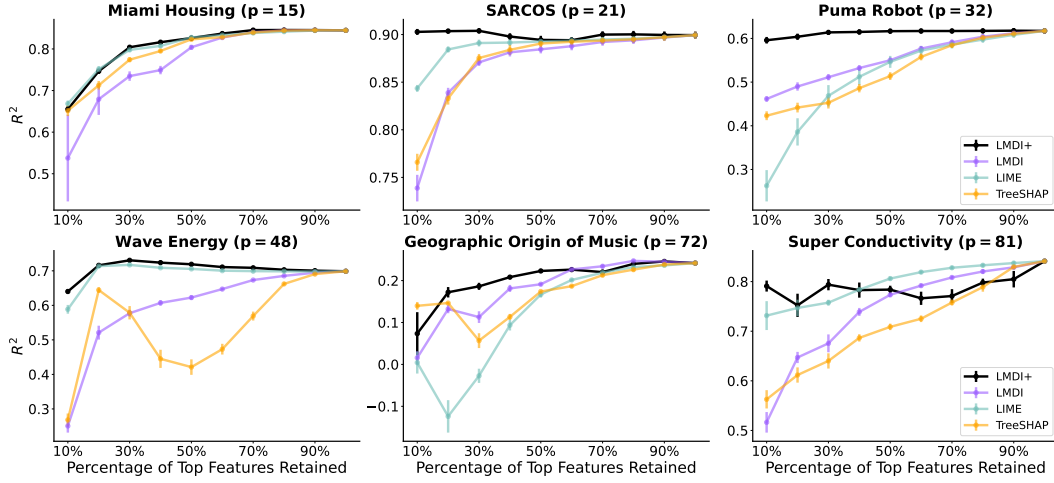


Figure 12: For regression benchmark datasets, LMDI+ achieves higher test R^2 after retraining on the masked training data selected by its feature ranking, demonstrating its ability to identify more signal features than baseline methods. Results are averaged over 20 runs with different random sampling and train-test splits. Error bars indicate the standard error of the mean.

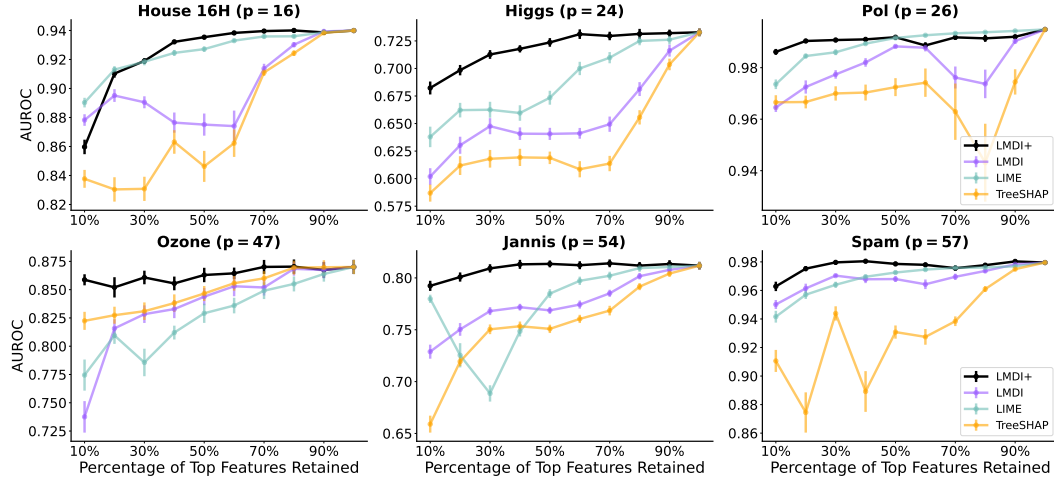


Figure 13: For classification benchmark datasets, LMDI+ achieves higher test AUROC after retraining on the masked training data selected by its feature ranking, demonstrating its ability to identify more signal features than baseline methods. Results are averaged over 20 runs with different random sampling and train-test splits. Error bars indicate the standard error of the mean.

F Stability Experiments Results

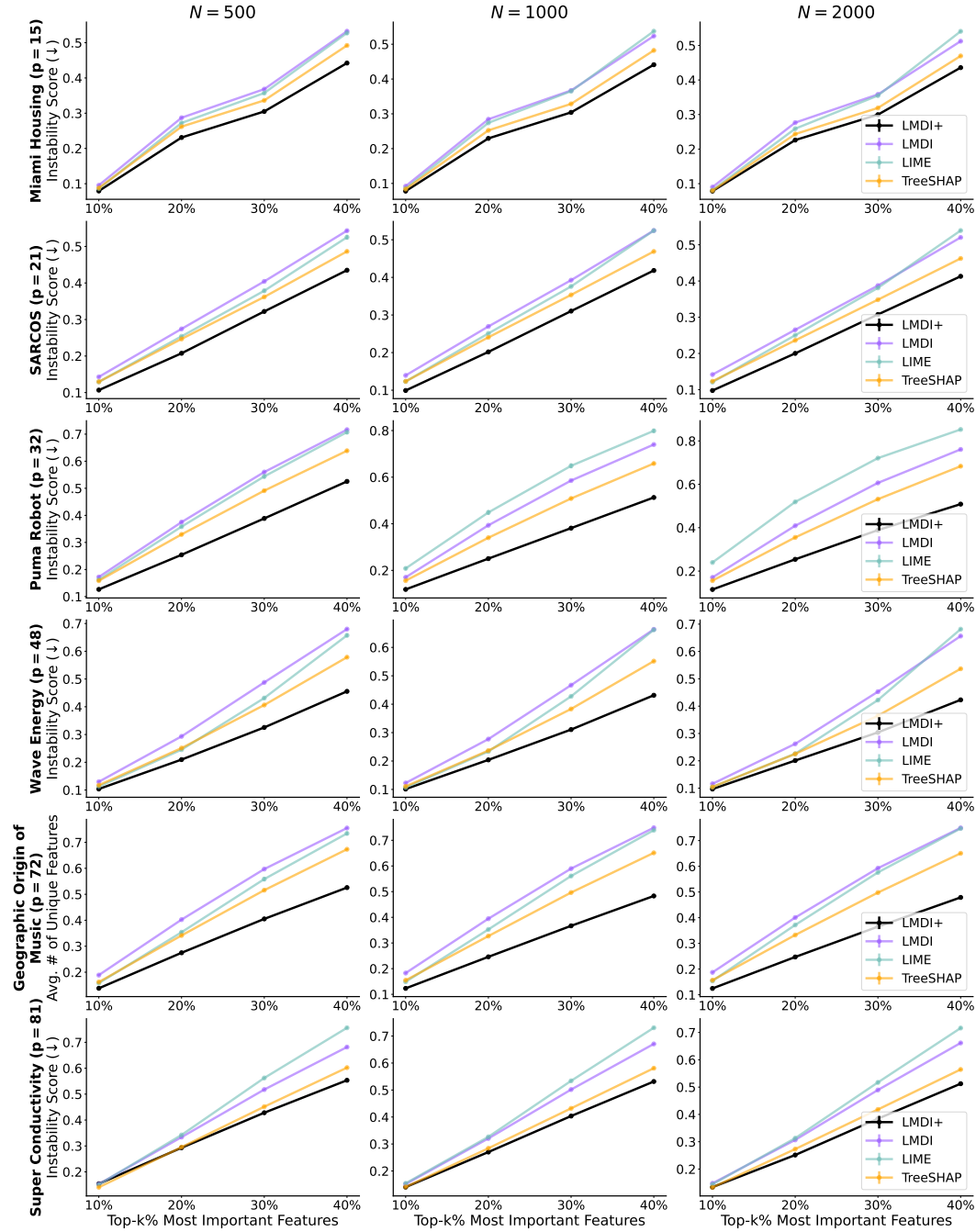


Figure 14: Across all regression benchmark datasets, LMDI+ yields more stable feature rankings as it identifies a smaller number of unique features compared to baselines when selecting the top important features across different random forest fits on the same data. Performance is reported as the average on the entire set and is averaged over 15 runs with different random sampling and train-test splits. Error bars showing the standard error of the mean.

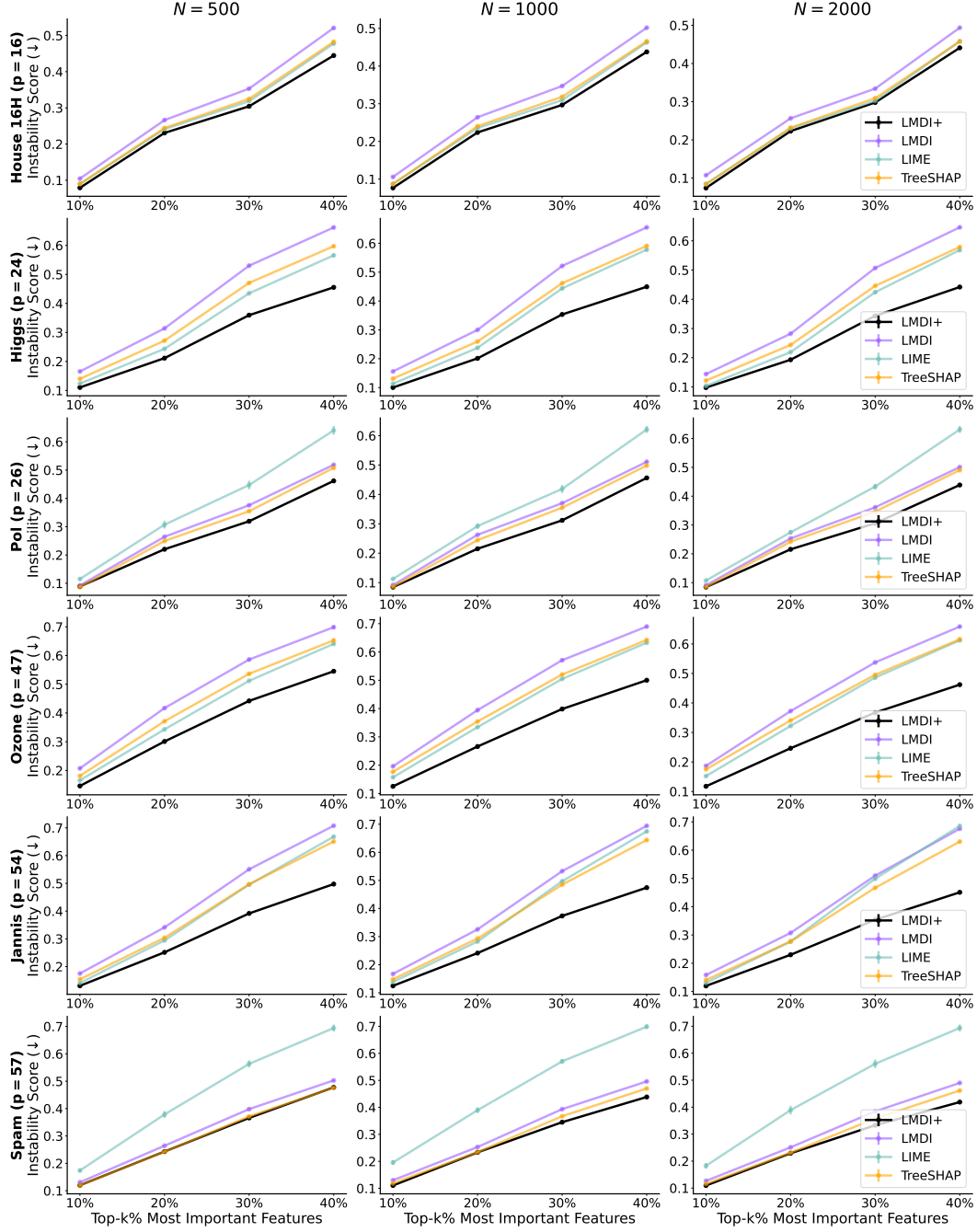


Figure 15: Across all classification benchmark datasets, LMDI+ yields more stable feature rankings as it identifies a smaller number of unique features compared to baselines when selecting the top important features across different random forest fits on the same data. Performance is reported as the average on the entire set and is averaged over 15 runs with different random sampling and train-test splits. Error bars showing the standard error of the mean.

G Counterfactuals on Local Feature Importance Prioritize Signal Features

G.1 Experiment Setup

For $i = 1, \dots, 2000$, we take $\mathbf{x}_i \sim \mathcal{N}_{10}(0, I_{10})$. We set coefficients $\beta = [5, 4, 3, 2, 1, 0, 0, 0, 0, 0]$ such that X_1, \dots, X_5 are signal features with X_1 being the strongest signal and X_6, \dots, X_{10} are noise features. We then generate labels \mathbf{y} by taking $\text{sign}(\mathbf{X}\beta + \epsilon)$, with $\epsilon = 0.1$. We note this is a high signal-to-noise ratio: a logistic regression model attains 99% accuracy on held-out data.

We fit a random forest to half of the data and compute local feature importances on both the training and held-out test data. We compute counterfactuals both by using the observed data and local feature importances as described in Section 7.

G.2 Results

In Figure 16 we show the distribution of coordinate-wise distances to the nearest counterfactual training observation. Note that features 1-5 are signal features with decreasing levels of signal. Thus, we want our counterfactual to be closest with respect to X_1 , then X_2 , and so on. We see that the counterfactuals found using the observed data tend to be closer with respect to the noise features X_6, \dots, X_{10} . Meanwhile, the local feature importance methods find counterfactuals that are closest with respect to signal features, with the distance increasing as signal lessens.

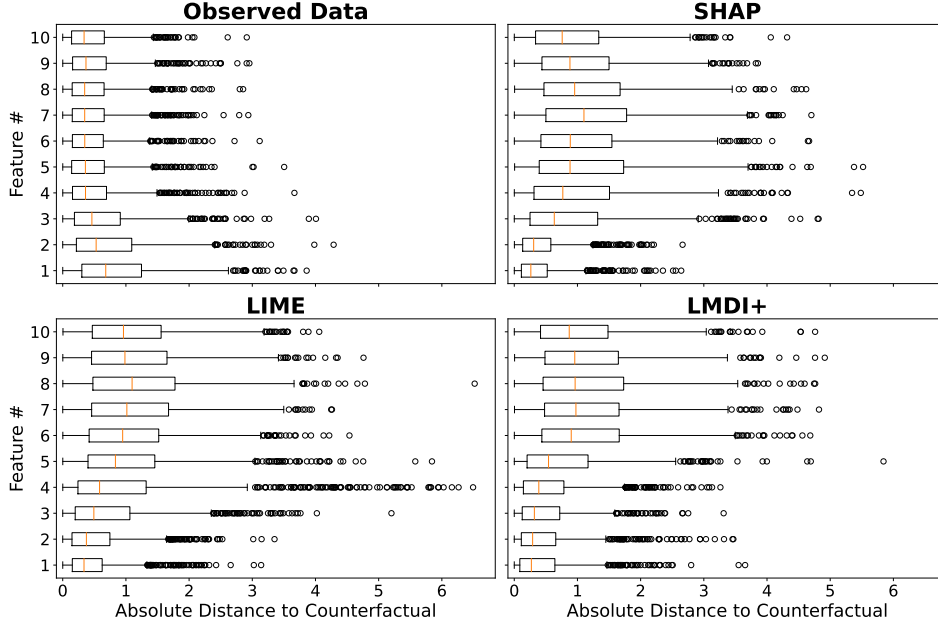


Figure 16: Distribution of coordinate-wise distances between an observation and its counterfactual. When using local feature importance space to find the closest counterfactual, the detected explanation is more similar with respect to signal features. Using the observed data, which is the typical approach, instead results in counterfactual explanations that are more similar with respect to noise features.

H Exploratory Subgroup Analysis

In this section, we investigate the patterns within the subgroups formed by LMDI+. We select $k = 4$ clusters using the stability method described in Algorithm 1 of Ben-Hur et al. [53]. We begin by visualizing the cluster on a map of Miami, which can be seen in Figure 17. We witness a clear geographic trend, with cluster 4 containing the houses closest to the city center, cluster 2 containing the houses in wealthy suburbs such as Coral Gables, Pinecrest, and Palmetto Bay, and clusters 1 and 3 containing the houses in the outlying suburbs of Miami-Dade County.

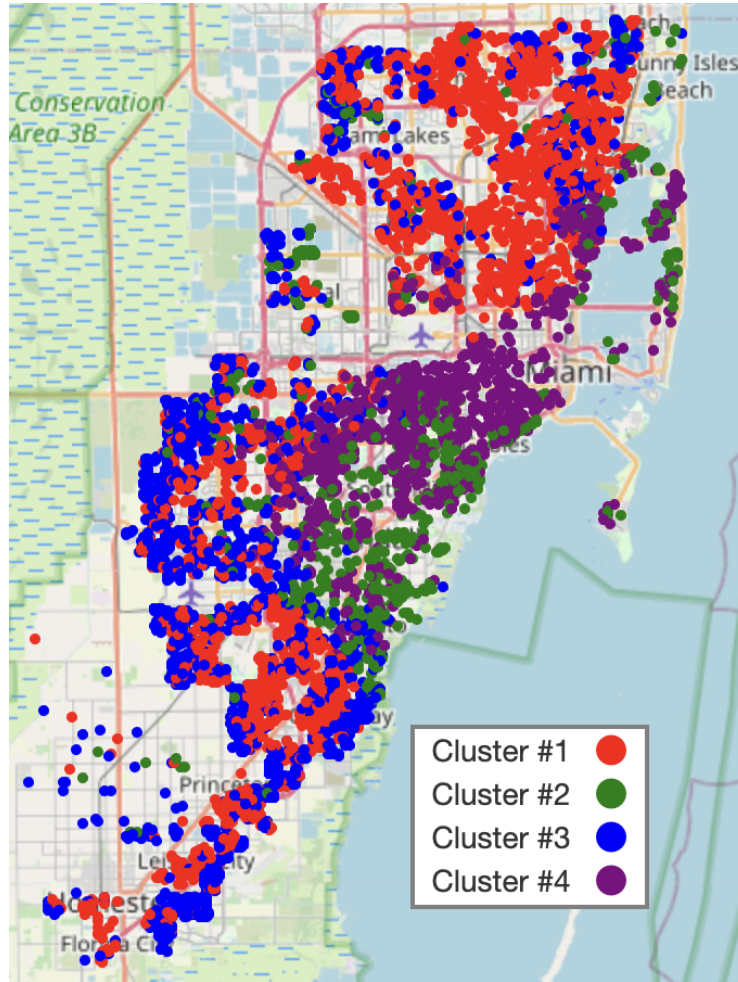


Figure 17: Homes in Miami-Dade County, location determined by latitude and longitude. We witness clear geographic trends, with Cluster 1 and 3 comprising the outer suburbs, Cluster 2 comprising of the wealthier coastal suburbs, and Cluster 4 containing the homes closer to the city center.

The left side of Figure 18 allows us to examine living area, a key driver of house prices. We observe a clear separation between clusters 1 and 3, implying that subgroup 1 contains the smaller suburban homes than subgroup 3, allowing us to differentiate between them. Investigating home price by cluster, which can be seen on the right side of Figure 18, completes the story. We see that homes in cluster 1 are the least expensive, likely due to a combination of their size and distance from the city center. Despite their similar location to cluster 1, homes in cluster 3 consistently sell for higher prices due to their larger nature. Finally, we see that homes in cluster 4 are valuable due to their proximity to the city center, while homes in cluster 2 are valuable due to their large size.

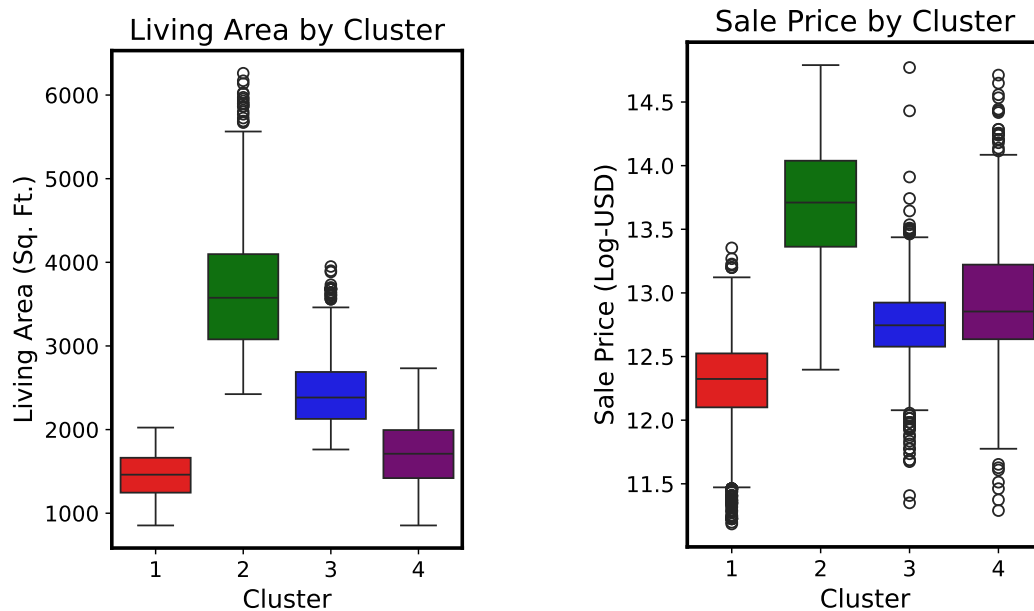


Figure 18: We observe that the distributions of living area and home price differ drastically between clusters, indicating key characteristics of each group.